MOLECULAR IMAGING AND BIOLOGY

Mol Imaging Biol (2019) 21:917–925
DOI: 10.1007/s11307-019-01316-7

Published Online: 4 February 2019

RESEARCH ARTICLE

Glucose-6-phosphatase Expression–Mediated [^{18}F]FDG Efflux in Murine Inflammation and Cancer Models

Mi Jeong Kim,[1,2,3] Chul-Hee Lee,[1,4] Youngeun Lee,[1,5] Hyewon Youn,[1,2,3,6] Keon Wook Kang,[1,2,4] JoonHo Kwon,[1,7] Abass Alavi,[8] Sean Carlin,[8] Gi Jeong Cheon,[1,2,5] June-Key Chung[1,2,3,4,9]

[1]*Department of Nuclear Medicine, Seoul National University College of Medicine, Seoul, South Korea*
[2]*Laboratory of Molecular Imaging and Therapy, Cancer Research Institute, Seoul National University College of Medicine, Seoul, South Korea*
[3]*Tumor Microenvironment Global Core Research Center, Seoul National University, Seoul, South Korea*
[4]*Biomedical Sciences, Seoul National University College of Medicine, Seoul, South Korea*
[5]*Tumor Biology Program, Seoul National University College of Medicine, Seoul, South Korea*
[6]*Cancer Imaging Center, Seoul National University Cancer Hospital, Seoul, South Korea*
[7]*Institute of Radiation Medicine, Seoul National University College of Medicine, Seoul, South Korea*
[8]*Division of Nuclear Medicine, Department of Radiology, Hospital of the University of Pennsylvania, Philadelphia, PA, USA*
[9]*Department of Nuclear Medicine, National Cancer Center, Goyang, Republic of Korea*

Abstract

Purpose: 2-Deoxy-2-[^{18}F]fluoro-D-glucose ([^{18}F]FDG) accumulation in inflammatory lesions can confound the diagnosis of cancer. In this study, we investigated [^{18}F]FDG accumulation and efflux in relation to the genes and proteins involved in glucose metabolism in murine inflammation and cancer models.

Procedures: [^{18}F]FDG accumulation and [^{18}F]FDG efflux were measured in cancer cells (breast cancer, glioma, thyroid cancer, and hepatoma cells) and RAW 264.7 cells (macrophages) activated with lipopolysaccharide (LPS). The levels of mRNA expression were measured by real-time quantitative PCR (qPCR). The expression of glucose metabolism–related proteins was detected by western blotting. Dynamic [^{18}F]FDG positron emission tomography-computed tomography (PET/CT) images were acquired for 2 h in tumor-bearing BALB/c nude mice and inflammatory mice induced by turpentine oil.

Results: [^{18}F]FDG accumulation in MDA-MB-231 (breast cancer) increased with time, but that of HepG2 (hepatoma) reached a constant level after 120 min. [^{18}F]FDG efflux in HepG2 was faster than that in MDA-MB-231. HepG2 strongly expressed glucose-6-phosphatase (G6Pase) compared with MDA-MB-231. [^{18}F]FDG accumulation increased with time, and [^{18}F]FDG efflux accelerated after the activation of RAW 264.7 cells. The expression levels of G6Pase, glucose transporter1 and glucose transporter3 (GLUT1 and GLUT3), and hexokinase II (HK II) increased after the activation of RAW 264.7 cells. [^{18}F]FDG efflux in activated

Mi Jeong Kim, Chul-Hee Lee and Youngeun Lee contributed equally to this research.

Electronic supplementary material The online version of this article (https://doi.org/10.1007/s11307-019-01316-7) contains supplementary material, which is available to authorized users.

Correspondence to: Abass Alavi; *e-mail:* Abass.Alavi@uphs.upenn.edu, June-Key Chung; *e-mail:* jkchung@snu.ac.kr

macrophages was faster than that in MDA-MB-231 cancer cells. MDA-MB-231 strongly expressed HK II protein compared with the activated RAW 264.7. In murine models, [18F]FDG accumulation in MDA-MB-231 cancer and inflammatory lesions increased with time, but that in HepG2 tumor increased until 20–30 min (SUVmeans ± SD (tumor/muscle), 3.0 ± 1.3) and then decreased (2.1 ± 0.9 at 110–120 min).

Conclusions: There was no difference in the pattern of [18F]FDG accumulation with time in MDA-MB-231 tumors and inflammatory lesions. We found that [18F]FDG efflux accelerated in activated macrophages reflecting increased G6Pase expression after activation and lower expression of HK II protein than that in MDA-MB-231 cancer cells.

Key words: 2-Deoxy-2-[18F]fluoro-D-glucose ([18F]FDG), Positron emission tomography (PET), Inflammation, Cancer, Glucose-6-phosphatase (G6Pase)

Introduction

2-Deoxy-2-[18F]fluoro-D-glucose ([18F]FDG) positron emission tomography (PET) has been widely applied for the diagnosis of various cancers due to the high demand for glycolysis in tumors [1, 2]. [18F]FDG, as a glucose analogue, is transported by glucose transporters (GLUTs) into cells, where it can then be phosphorylated by hexokinase (HK) [3]. The [18F]FDG-6-phosphate ([18F]FDG-6P) accumulates within the cell as a terminal metabolite without exiting from the cell, but it does not continue down the glycolytic pathway. However, [18F]FDG-6P can be dephosphorylated by glucose-6-phosphatase (G6Pase) to [18F]FDG, which can then efflux from the cell. Therefore, [18F]FDG uptake and efflux in cancer cells are related to the expression and activity of glucose metabolism–related proteins. High [18F]FDG accumulation has been reported in many human tumors overexpressing glucose transporter1 (GLUT1) and hexokinase II (HK II) [4–6]. A study showed that low [18F]FDG accumulation in hepatocellular carcinoma (HCC) was related to high G6Pase expression [7].

[18F]FDG is also accumulated in inflammatory cells [8–11]. In fact, [18F]FDG accumulation in inflammatory lesions confounds the diagnosis of cancer. Some researchers suggested [18F]FDG imaging method of dual time-point to differentiate inflammation and cancer, according to differences in [18F]FDG retention [12, 13]. However, other investigators have reported overlaps in the retention [14–16]. To solve the discrepancy, a few studies compared glucose-related gene expressions between cancer and inflammation. However, there were limited data resulting no consensus on this issue. In this study, we assessed the [18F]FDG accumulation and efflux patterns in murine cancer and inflammation mouse models. To elucidate the mechanisms of [18F]FDG accumulation, we analyzed the expression of glucose metabolism–related genes and proteins.

Materials and Methods

Cell Cultures and Activation of Macrophages

A human breast cancer cell line (MDA-MB-231), a human hepatoma cell line (HepG2), and a murine macrophage cell line (RAW 264.7) were obtained from American Type Culture Collection (ATCC, Manassas, VA, USA). MDA-MB231 and RAW 264.7 cells were cultured in Dulbecco's modified Eagle medium (DMEM; Welgene, Gyeongsan-si, Republic of Korea), and HepG2 cells were cultured in Eagle's minimum essential medium (EMEM; ATCC). The culture media contained heat-inactivated 10 % fetal bovine serum (Thermo Fisher Scientific, Waltham, MA) and 1× antibiotic-antimycotic solution (Thermo Fisher Scientific) or penicillin streptomycin (Thermo Fisher Scientific) at 37 °C in a 5 % CO_2 humidified atmosphere. For the activation of RAW 264.7 cells, 2×10^5 RAW 264.7 cells in six-well plates were stimulated with 100 ng/ml lipopolysaccharide (LPS; Sigma-Aldrich, St. Louis, MO) for 24 h or for different times.

[18F]FDG Accumulation Assay

2×10^5 cells/well were plated in six-well plates and pre-incubated with glucose-free RPMI medium (Thermo Fisher Scientific) for 4 h. The cells were incubated with 185 kBq of [18F]FDG in Hank's balanced salt solution (HBSS; Thermo Fisher Scientific) buffer for 10, 30, 60, 120, 240, and 360 min at 37 °C. The cells were washed twice in ice-cold HBSS buffer and then dissolved in 1 % sodium dodecyl sulfate (SDS) buffer. The radioactivity of the lysates was measured using a γ-counter (Canberra-Packard, Meriden, CT). Experiments were performed in triplicate. All samples were normalized by protein concentration (mg) using a BCA protein assay kit (Thermo Fisher Scientific).

[18F]FDG Efflux Assay

2×10^5 cells/well were plated in six-well plates and pre-incubated with glucose-free RPMI medium for 4 h. The cells were rinsed in 1 ml of HBSS buffer and incubated with 185 kBq of [18F]FDG in HBSS buffer for 1 h at 37 °C. The cells were washed twice in cold HBSS and incubated in fresh media for various times (10, 20, 30 (or 50), 90 (or 80), and 120 (or 110) min). The media were harvested. Finally, the cells were washed twice in cold HBSS buffer and then dissolved in 1 ml of 1 % SDS buffer. The radioactivity of the supernatants and the cell lysates was measured using a γ-counter. Experiments were performed in triplicate. The data showed radioactivity remaining in the cells, calculated as the radioactivity of each supernatant and cell lysate at the final time point. $T_{1/2}$ of the [18F]FDG efflux was calculated for the time required until a reduction to half from the [18F]FDG accumulated for 1 h.

Western Blot

Cells were lysed in radio-immunoprecipitation assay (RIPA) buffer (Sigma-Aldrich) containing a protease inhibitor cocktail (Roche Diagnostics, Basel, Switzerland). Protein concentrations were measured using a BCA protein assay kit (Thermo Fisher Scientific). Protein samples were separated using a NuPAGE Bis-Tris Gel (Thermo Fisher Scientific) and were transferred to PVDF membranes (Millipore, Billerica, MA). The PVDF membranes were blocked in 5 % skim milk (*w*/*v*) for 1 h at room temperature (RT). Membranes were incubated overnight at 4 °C with primary antibodies against GLUT1 (1:1000 dilution; Abcam, Cambridge, MA), glucose transporter3 (GLUT3) (1:400 dilution; Abcam), HK II (1:1000 dilution; Cell Signaling Technology, Danvers, MA), G6Pase (1:1000 dilution; Abcam), or β-actin (1:5000 dilution; Sigma-Aldrich). Membranes were incubated with a secondary anti-rabbit or anti-mouse horseradish peroxidase–conjugated antibodies (Cell Signaling Technology, Danvers, MA). Immunoreactive bands were visualized using ECL reagents (Roche) and detected using the LAS-3000 system (FUJIFILM, Stockholm, Sweden). Target proteins were normalized to β-actin. Relative ratios of HK II or G6Pase expression levels in the activated RAW 264.7 cells were calculated compared with those in the inactivated RAW 264.7 cells after normalization against β-actin expression levels. Relative ratios of HK II and G6Pase expression levels in the MDA-MB-231 cells were calculated compared with those in the activated RAW 264.7 cells.

Immunohistochemistry

Tumor and inflammation tissues were embedded in paraffin, and were cut in 4-μm-thick sections. After xylene treatment, the tissue sections were rehydrated. The sections were heated using a microwave in 10 mM sodium citrate buffer for 8 min, and blocked with goat serum (1:30 dilution; Vector Laboratories Ltd., Burlingame, CA). The sections were incubated with macrophage-specific antibodies against F4/80 (1:50 dilution; Cat. No. ab6640, Abcam, Cambridge, UK) overnight at 4 °C. After washing, the tissue sections were incubated with biotinylated secondary anti-rat antibodies for 1 h, and again incubated with the Elite ABC kit reagent (Vector Laboratories Ltd., Burlingame, CA). The sections were incubated with a 3,3′- diaminobenzidine peroxidase substrate solution (Vector Laboratories Ltd., Burlingame, CA) followed by Mayer's hematoxylin counterstaining (Sigma-Aldrich, St. Louis, MO). As negative controls, the sections were incubated with isotype control rat IgG instead of the primary antibodies. We examined the tissue sections under a light microscope after Permount mounting.

Mouse Models of Tumor and Inflammation

BALB/c nude mice (male, 6 weeks old) were used in accordance with the Institutional Animal Care and Use Committee (IACUC) of Seoul National University Hospital guidelines. Five million MDA-MB-231 cells ($N = 4$) or ten million HepG2 cells ($N = 4$) in 50 μl of Matrigel (BD Biosciences, Bedford, MA) were implanted subcutaneously into the left front thigh. When the tumor diameters reached 6.1~11.4 mm, the mice were used for the experiments. In a different group of mice, inflammation ($N = 4$) was induced in the right front thigh by an intramuscular (IM) injection of 50 μl of turpentine oil 3 days prior to PET imaging [14, 17], and 50 μl of PBS was injected in the left front thigh as a control.

Dynamic [18F]FDG PET Imaging

Prior to the [18F]FDG PET imaging, the mice were fasted for at least 6 h to minimize the competitive inhibition by serum glucose. Following intravenous injection of 11.0–16.6 MBq of [18F]FDG, dynamic PET images were acquired for 2 h using an animal PET/CT scan (eXplore Vista CT; GE Healthcare, Waukesha, USA). A 32-frame dynamic protocol (4 × 3 s, 8 × 6 s, 8 × 30 s, 1 × 300 s, 11 × 600 s) was used for the emission PET scans [18]. The AMIDE (Amide's Medical Imaging Data Examiner) software was used to view the [18F]FDG PET images. Volume of interest (VOI) of the PET images was analyzed to 20 % of the maximal VOI signal using PMOD software (PMOD Technologies). The mean standardized uptake value (SUVmean) and standard deviation (SD) were obtained, and the tumor-to-muscle (*T*/*M*) ratios or the inflammation-to-muscle (*I*/*M*) ratios were calculated.

Statistical Analysis

Data are shown as the mean ± standard deviation. Statistical comparisons were analyzed on the groups using Student's *t* test and the Mann-Whitney *U* test with SPSS software version 23 (IBM Corporation, Chicago, IL). A *p* value of less than 0.05, 0.01, or 0.001 was considered statistically significant.

Results

[18F]FDG Accumulation and Expression of Glucose Metabolism–Related Proteins in Cancer Cells

[18F]FDG accumulation by various cancer cells (breast cancer (MCF-7 and MDA-MB-231), glioma (U87MG and U373), and thyroid cancer (TPC-1 and FRO) cells) increased over time, but that of hepatoma cells (Hep3B and HepG2) reached a constant level after 120 min (see Suppl. Fig. 1 in Electronic Supplementary Material (ESM)). To demonstrate association of [18F]FDG accumulation pattern and glucose metabolism–related mechanism, we chose two cancer cell lines (MDA-MB-231 and HepG2 cells) with two different patterns of [18F]FDG accumulation. [18F]FDG accumulation by MDA-MB-231 cells increased continuously until 360 min, but that of HepG2 cells reached a constant level after 120 min (Fig. 1a). $T_{1/2}$ of [18F]FDG efflux (116 min) in MDA-MB-231 cells took 1.8 times longer (64 min) than that in HepG2 cells (Fig. 1b).

The mRNA expression of GLUT1, HK II, and G6Pase in HepG2 cells was 13.4-fold, 2.3-fold, and 385.8-fold higher, respectively, than that in MDA-MB-231 cells (Suppl. Fig. 2 in ESM). We found that the expression of G6Pase protein in HepG2 cells was much higher than that in MDA-MB-231 cells (Fig. 1c). These results showed that higher [18F]FDG accumulation in MDA-MB-231 cells was due to the high expression of HK II and very low expression of G6Pase, and fast [18F]FDG efflux in HepG2 cells was due to the strong expression of G6Pase, despite the high expression of GLUT1 and HK II.

[18F]FDG Accumulation and Expression of Glucose Metabolism–Related Proteins in Activated Macrophages

To study the condition of inflammation, RAW 264.7 cells were activated with LPS, and their morphological changes were observed (suppl. Fig. 3a in ESM). Pro-inflammatory cytokines such as TNF-α, IL-1β, and IL-6 in the activated RAW 264.7 cells significantly increased (suppl. Fig. 3b–d in ESM). We confirmed that RAW 264.7 cells were activated by treatment with LPS.

[18F]FDG accumulation in the activated RAW 264.7 cells was higher than that in the inactivated RAW 264.7 cells (Fig. 2a). [18F]FDG accumulation in the activated RAW 264.7 cells increased until 240 min, and then subsequently decreased at later time points. $T_{1/2}$ of [18F]FDG efflux (69 min) in inactivated RAW 264.7 cells took 1.4 times longer (50 min) than that in activated RAW 264.7 cells (Fig. 2b).

mRNA expression of GLUT1, HK II, and G6Pase increased after activation of RAW 264.7 cells, although G6Pase gene expression was low, and there was no statistically significant difference (Supple. Fig. 4 in ESM). The expression of GLUT1 and GLUT3, major isomers of glucose transporters; HK II protein; and G6Pase protein increased after the activation of RAW 264.7 cells (Fig. 2c). The ratios of increased HK II protein expression (6.0-fold) compared with inactivated RAW 264.7 cells were higher than those of G6Pase (2.1-fold) at 24 h after activation. These results showed increased [18F]FDG accumulation, reflecting the increase in glucose transporters and HK II expression, and accelerated [18F]FDG efflux, reflecting the increase in G6Pase expression after the activation of RAW 264.7 cells.

[18F]FDG Accumulation and Expression of Glucose Metabolism–Related Proteins in Macrophages and Cancer Cells

To demonstrate similar patterns of [18F]FDG accumulation in MDA-MB-231 cancer cells and activated RAW 264.7 cells, we compared the [18F]FDG accumulation in both cell lines. [18F]FDG accumulation in MDA-MB-231 cells was higher than that in activated RAW 264.7 cells (Fig. 3a). $T_{1/2}$ of [18F]FDG efflux (115 min) in MDA-MB-231 cells took 2.3 times longer (50 min) than that in activated RAW 264.7 cells (Fig. 3b).

The expression levels of HK II (2.0-fold) and G6Pase (3.6-fold) proteins in MDA-MB-231 cells were higher than those in the activated RAW 264.7 cells, although G6Pase expression increased after activation (Fig. 3c). These results showed the high [18F]FDG accumulation and slow [18F]FDG efflux in MDA-MB-231 cells, reflecting the strong expression of HK II despite a higher expression of G6Pase than that of the activated RAW 264.7 cells.

Dynamic [18F]FDG PET Findings in Murine Cancer and Inflammatory Models

[18F]FDG accumulation in MDA-MB-231 tumor–bearing mice increased over time (Fig. 4a, b). The SUVmeans ± SD (tumor/muscle) at 20–30, 50–60, 80–90, and 110–120 min were 1.4 ± 0.2, 2.2 ± 1.0, 2.4 ± 1.2, and 2.5 ± 1.3, respectively. However, the SUVmeans ± SD (tumor/muscle) in HepG2 tumor–bearing mice reached a constant level at 20–30 min (3.0 ± 1.3) and then decreased until 110–120 min (2.1 ± 0.9). [18F]FDG accumulation in the inflammatory lesion increased over time compared with PBS-injected

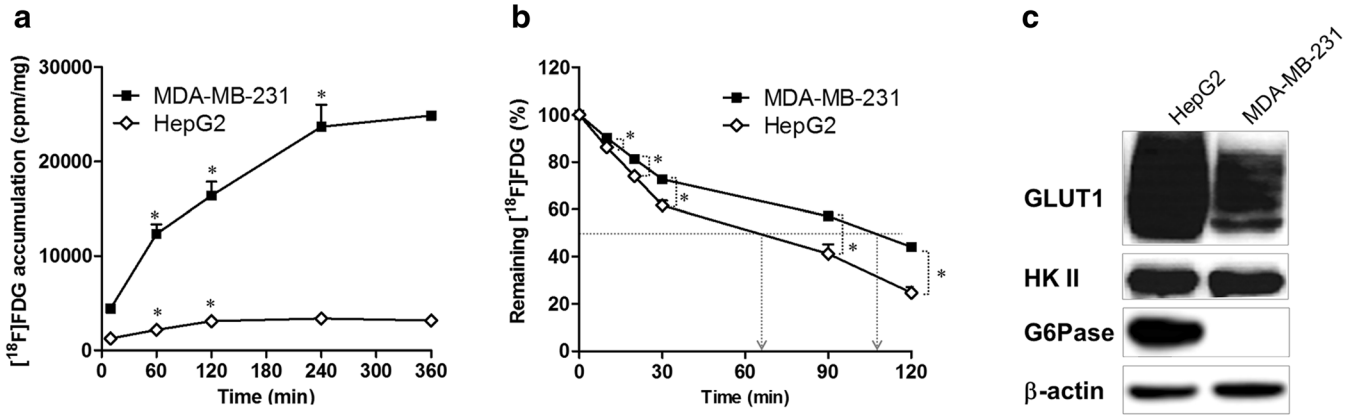

Fig. 1. [18F]FDG accumulation and efflux and expression of glucose metabolism–related proteins in MDA-MB-231 and HepG2 cells. **a** [18F]FDG accumulation and **b** [18F]FDG efflux were measured in MDA-MB-231 and HepG2 cells. *$p < 0.05$. All values are presented as the mean ± SD in triplicate. **c** The expression of glucose metabolism–related proteins, glucose transporter1 (GLUT1), hexokinase II (HK II), and glucose-6-phosphatase (G6Pase), was detected by western blotting.

control lesions. The SUVmeans ± SD (inflammation/muscle) in the inflammatory lesion at 20–30, 50–60, 80–90, and 110–120 min were 2.3 ± 0.5, 2.6 ± 0.6, 2.7 ± 0.7, and 2.8 ± 0.7, respectively. Histopathologic analysis confirmed that F4/80-positive macrophages were infiltrated between the muscle tissues in the inflammatory lesion (Fig. 4c). No histological change was observed in PBS-treated control muscles. These results showed that [18F]FDG accumulation in murine inflammatory lesions and MDA-MB-231 tumor increased as time goes by, and that in HepG2 tumors reached a constant level and then decreased.

Discussion

We assessed the pattern of [18F]FDG accumulation in murine cancer and inflammatory models, and we measured the expression of glucose metabolism–related genes and proteins to elucidate the mechanisms of [18F]FDG accumulation. [18F]FDG accumulation increased over time in murine cancer and inflammatory mouse models reflecting the upregulation of GLUT1 and HK II expressions. In addition, [18F]FDG efflux accelerated, reflecting the upregulation of G6Pase expression after the activation of macrophages and lower expression of HK II protein than in MDA-MB-231 cancer cells.

We thought that the different patterns of [18F]FDG accumulation in various cancer cells should be characterized. We first examined [18F]FDG accumulation patterns in various cancer cell lines, and then chose two cancer cell lines (MDA-MB-231 and HepG2) to show two different patterns of [18F]FDG accumulation. [18F]FDG accumulation in MDA-MB-231 cells and MDA-MB-231 tumor–bearing mice continuously increased. GLUT1 and HK II were expressed strongly in MDA-MB-231 cells. It has been

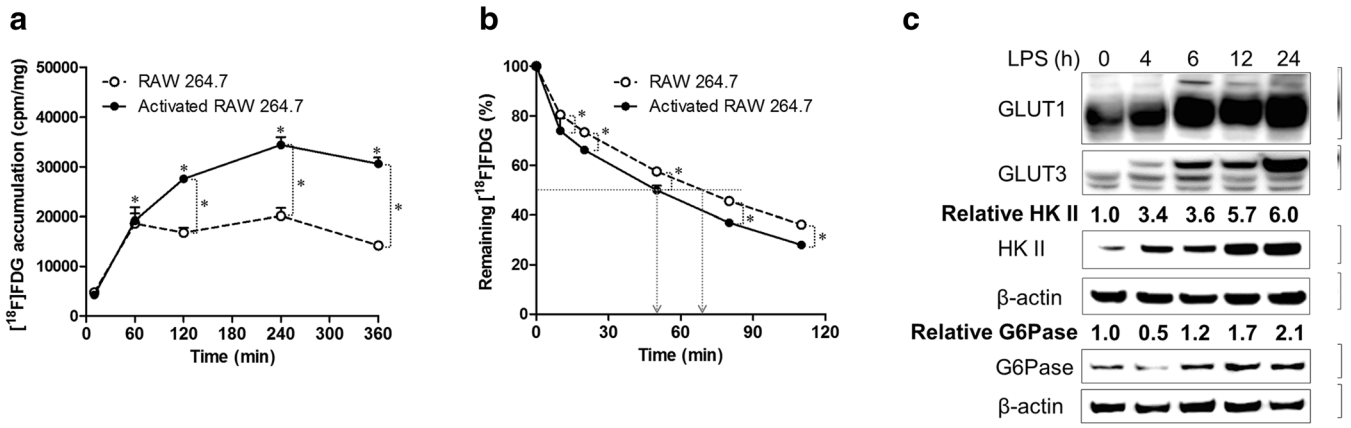

Fig. 2. [18F]FDG accumulation and efflux and expression of glucose metabolism–related proteins in activated RAW 264.7 cells. **a** [18F]FDG accumulation and **b** [18F]FDG efflux in inactivated RAW 264.7 cells and activated RAW 264.7 cells treated with LPS for 24 h. *$p < 0.05$. All values are presented as the mean ± SD in triplicate. **c** The expression of glucose metabolism–related proteins, glucose transporter1 (GLUT1), glucose transporter3 (GLUT3), hexokinase II (HK II), and glucose-6-phosphatase (G6Pase), was detected by western blotting.

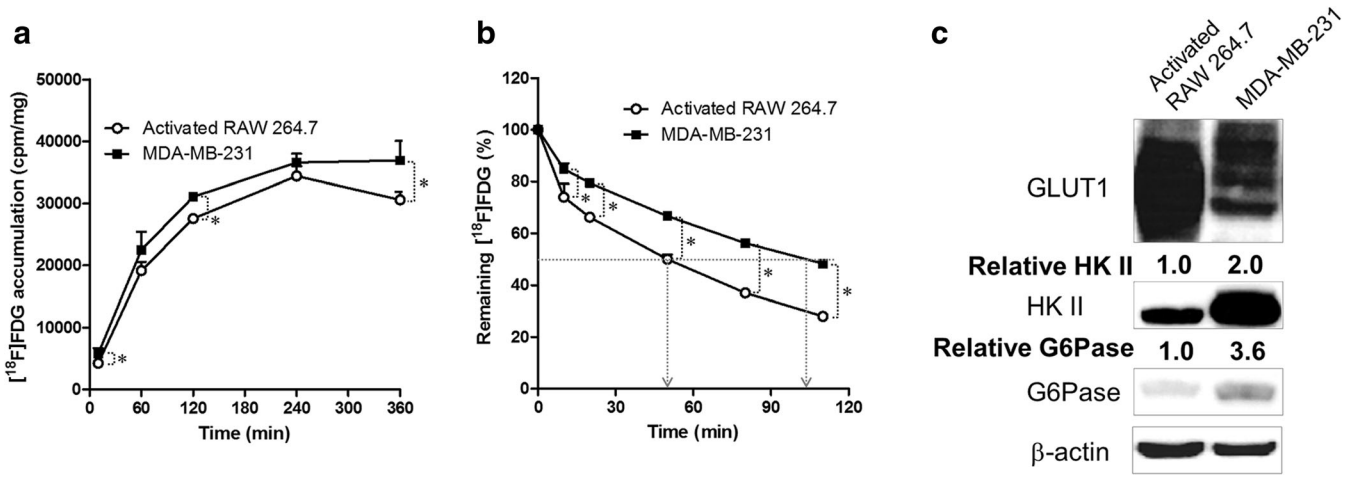

Fig. 3. [18F]FDG accumulation and efflux and expression of glucose metabolism–related proteins in activated RAW 264.7 and MDA-MB-231 cells. **a** [18F]FDG accumulation and **b** [18F]FDG efflux in activated RAW 264.7 with LPS for 24 h and MDA-MB-231 cells. $^{*}p < 0.05$. Values are presented as the mean ± SD in triplicate. **c** The expression of glucose metabolism–related proteins, glucose transporter1 (GLUT1), hexokinase II (HK II), and glucose-6-phosphatase (G6Pase), was detected by western blotting.

reported that [18F]FDG accumulation in cancer cells correlates with the expression of GLUT1 and hexokinase [3, 4]. Izuishi et al. reported that low [18F]FDG accumulation in moderately differentiated HCC reflected low GLUT1 and high G6Pase expression, while high [18F]FDG accumulation in poorly differentiated HCC could reflect increased GLUT1 and decreased G6Pase expression [7]. They showed that [18F]FDG accumulation in liver metastasis from colorectal cancer was higher than that in HCC. Their data of lower GLUT1 and HK levels and higher G6Pase levels in HCC than in hepatic metastases were suggested as rate-limiting factors for [18F]FDG accumulation. [18F]FDG efflux in hepatic metastases may be relatively slower than that in HCC because of higher G6Pase levels in HCC. The rate-limiting factors for [18F]FDG accumulation in HCC correspond to both slower [18F]FDG uptake and faster [18F]FDG efflux than hepatic metastases. In our data, [18F]FDG accumulation in HepG2 cells was saturated at an early time point, and [18F]FDG accumulation in HepG2 tumor–bearing mice reached a constant level at an early time point and then decreased. We found that these results reflected the strong expression of G6Pase protein, despite the high expression of GLUT1 and HK II. Further study needs to prove it; however, better or more [18F]FDG in hepatoma similar to HepG2 cells with overexpressed GLUT1 and HK as well as G6Pase levels may be expected if we image it at 20–30 min after injection of [18F]FDG.

In this study, [18F]FDG accumulation increased over time in the activated macrophages and in inflammatory lesions of the murine inflammatory models. We detected that GLUT1 and HK II expressions increased after activation of macrophages. Similar to our results, Satomi et al. reported that [18F]FDG uptake in THP-1 human origin M1 macrophages activated with LPS and IFN-γ increased, and mRNA expression of GLUT1 and HK II increased [19]. Similar to our results, Ren-Shyan Liu et al. reported that %ID/g of [18F]FDG accumulation in the inflammation-to-muscle increased over time until 4 h in the biodistribution data of turpentine oil–induced mouse models [14].

However, FDG accumulation pattern was different between experiments even in the same turpentine-induced inflammation model. For example, Ren et al. showed that [18F]FDG uptake in turpentine-induced murine inflammatory lesions steadily increased over time [15]. On the other hand, Yamada et al. reported that [18F]FDG accumulation in turpentine-induced inflammatory tissue increased gradually until 60 min post-injection and then decreased [17]. The different results of [18F]FDG accumulation may have occurred because of various *in vivo* factors, *e.g.*, blood supply, lesion architecture, or cellular activation, that influence [18F]FDG accumulation. Environmental factors can affect glucose accumulation parameters. It has been well known that the pH is lower in hypoxic tumors and in inflamed tissues. Recently, a significant correlation was reported between tumor pH and [18F]FDG uptake, as a high [18F]FDG uptake corresponds to lower extracellular pH values [20]. It has been reported that GLUT1 and HK levels related to [18F]FDG uptake increased in hypoxic tumor [21–23]. Amandine G et al. reported that glucotoxicity induced G6Pase catalytic unit expression by acting on the interaction of HIF-1α with the cAMP-response element–binding protein (CREB) on the G6Pase promoter in HepG2 cells [24]. [18F]FDG efflux regulated by G6Pase may be affected under intratumoral low pH in hypoxic tumor or inflamed tissues. In addition, we found accelerated [18F]FDG efflux after the activation of macrophages. We confirmed that protein expression of G6Pase increased after macrophage activation. We observed a slight decrease of [18F]FDG accumulation at

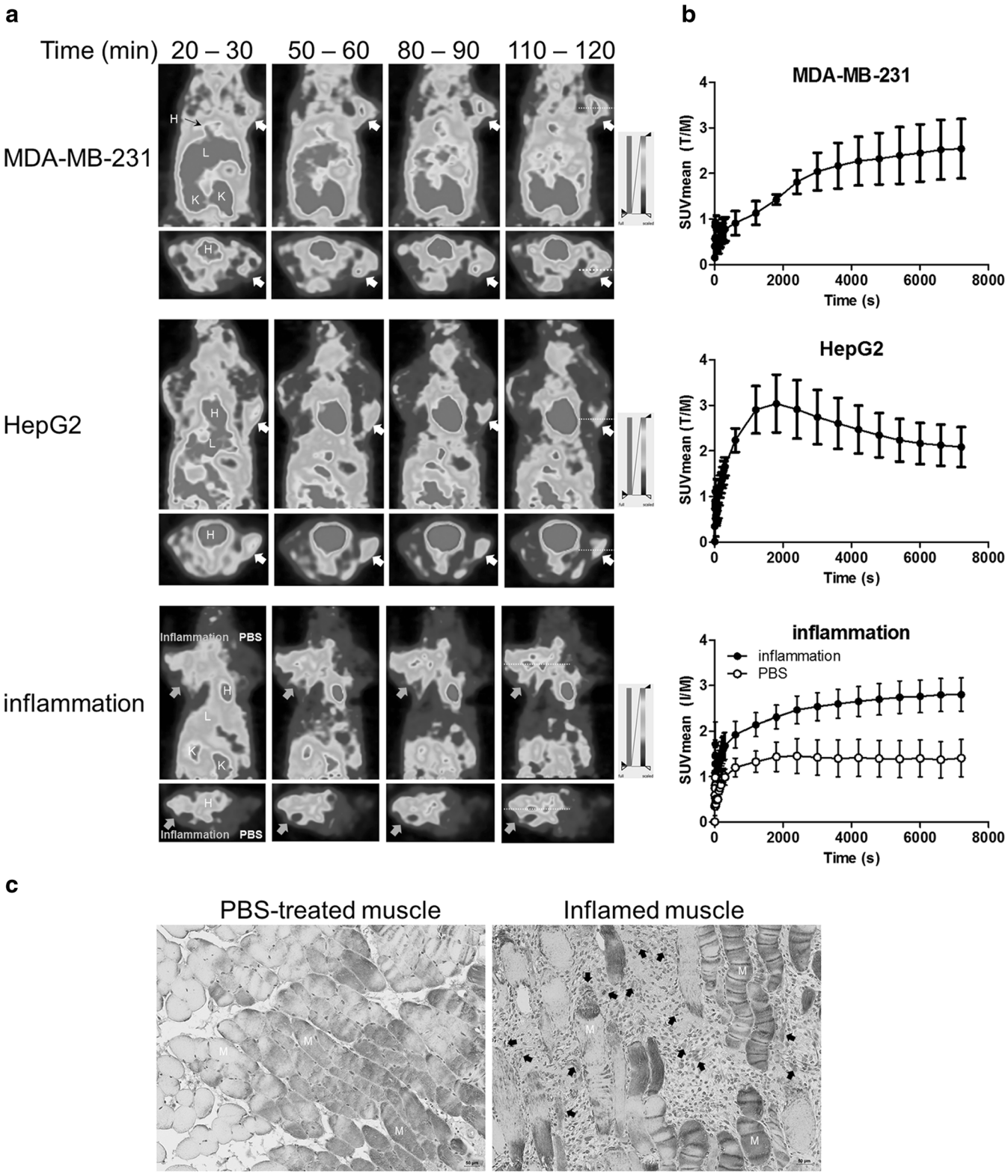

Fig. 4. Dynamic [18F]FDG PET imaging in cancer and inflammatory mouse models. **a** Representative coronal and transverse [18F]FDG PET images at 20–30, 50–60, 80–90, and 110–120 min in MDA-MB-231, HepG2, and inflammatory mouse models. Cancer and inflammatory lesions are indicated with white arrows and orange arrows, respectively. H, heart; L, liver; K, kidney. **b** Time-activity curves of [18F]FDG accumulated in MDA-MB-231 and HepG2 tumors, and inflammatory lesions. T/M, tumor-to-normal muscle; I/M, inflammation-to-normal muscle. **c** Histopathologic analysis of the inflamed muscle and PBS-treated muscle using immunohistochemistry with F4/80 macrophage antibodies. F4/80-positive macrophages are indicated with black arrows. M, muscle fibers. Scale bars represent 50 μm.

delayed time points in activated macrophages. The increase of dephosphorylation of [18F]FDG-6-phosphate by upregulated G6Pase in activated macrophages accelerated the [18F]FDG efflux and may have contributed to the slight decrease in [18F]FDG accumulation at delayed time points.

Several previous studies reported [18F]FDG accumulation in cancer and inflammatory models, but studies comparing their underlying mechanisms have, to our knowledge, not been reported yet. In our results, [18F]FDG accumulation in MDA-MB-231 cells was significantly higher than that in activated RAW 264.7 cells. This makes sense because HK II expression in MDA-MB-231 cells was higher than that in activated RAW 264.7 cells. [18F]FDG efflux in the activated macrophages was faster than that in the MDA-MB-231. Contrary to our expectations, G6Pase expression in MDA-MB-231 cells was higher than in activated RAW 264.7 cells. However, we found that HK II protein in MDA-MB-231 cells was strongly expressed. Therefore, the role of HK II may be even more dominant. Some researchers have suggested dual time-point imaging to distinguish malignant lesions from inflammatory lesions to enhance the diagnostic accuracy of [18F]FDG PET [12, 13, 25, 26]. Zhuang et al. showed that SUVs of inflammatory lesions on 90-min images decreased compared with those on 45-min images, whereas SUVs of tumors on 90-min images were significantly higher than those on 45-min images in rat models [12]. Hustinx et al. suggested dual time-point imaging as a clinical study protocol for differentiating malignant lesions of the patients with head and neck cancer from inflammatory lesions [25]. However, Kaneko et al. reported that [18F]FDG-avid benign pulmonary lesions (BPLs) showed high retention indexes (RIs), and no significant difference with primary lung cancer (PLC) RIs was found [16]. There exist significant differences in various aspects of the dual time-point PET imaging studies, which may contribute to the conflicting results reported in the literature. The reasons for the conflicting results may be due to the differences according to cancer type, cancer heterogeneity, the state of cancer progression, and the state of inflammation consisting of various inflammatory cells. Another reason for the conflicting results is the variation in the initial and delayed time points selected for image acquisition between studies [27–30].

Conclusions

In this study, we evaluated the expression levels of glucose accumulation parameters including GLUT, HK II, and G6Pase, and compared with the pattern of [18F]FDG accumulation. There was no difference in the pattern of [18F]FDG accumulation with time in MDA-MB-231 tumors and inflammatory lesions. [18F]FDG accumulation increased over time in MDA-MB-231 cancer and inflammatory mouse models. However, [18F]FDG efflux was accelerated in activated macrophages. Concurrently, we found upregulated G6Pase expression in the activated macrophages and lower expression of HK II protein than in MDA-MB-231 cancer cells. These kinds of knowledge will be useful for understanding pathophysiology and developing theranostics in both sides of carcinoma and inflammation.

Acknowledgements. We thank Professor Jae Sung Lee and Seung Kwan Kang for the support of dynamic [18F]FDG PET imaging, and Young Ju Kim for technical assistant of mouse PET imaging.

Funding. This work was supported by internal research funds from the Seoul National University Cancer Research Institute (cri-15-4, cri-16-3, and cri-17-3) and grants of the Korea Health Technology R&D Project through the Korea Health Industry Development Institute (KHIDI) funded by the Ministry of Health and Welfare (grant numbers HI14C1072 and HI14C1277); the National Research Foundation of Korea (NRF) grant for the Global Core Research Center (GCRC) funded by the Korea government Ministry of Science, ICT and Future Planning (MSIP) (No. 2011-0030001) (2017-R1A2B4012813); and Basic Science Research Program through the National Research Foundation of Korea (NRF) funded by the Ministry of Education (2009-0093820).

Compliance with Ethical Standards

Conflict of Interest

The authors declare that they have no conflict of interest.

References

1. Rigo P, Paulus P, Kaschten BJ, Hustinx R, Bury T, Jerusalem G, Benoit T, Foidart-Willems J (1996) Oncological applications of positron emission tomography with fluorine-18 fluorodeoxyglucose. Eur J Nucl Med 23:1641–1674
2. Bomanji JB, Costa DC, Ell PJ (2001) Clinical role of positron emission tomography in oncology. Lancet Oncol 2:157–164
3. Haberkorn U, Ziegler SI, Oberdorfer F, Trojan H, Haag D, Peschke P, Berger MR, Altmann A, van Kaick G (1994) FDG uptake, tumor proliferation and expression of glycolysis associated genes in animal tumor models. Nucl Med Biol 21:827–834
4. Ong LC, Jin Y, Song IC, Yu S, Zhang K (2008) 2-[18F]-2-deoxy-D-glucose (FDG) uptake in human tumor cells is related to the expression of GLUT-1 and hexokinase II. Acta Radiol 49:1145–1153
5. Smith TA (1999) Facilitative glucose transporter expression in human cancer tissue. Br J Biomed Sci 56:285–292
6. Adams V, Kempf W, Hassam S, Briner J (1995) Determination of hexokinase isoenzyme I and II composition by RT-PCR: increased hexokinase isoenzyme II in human renal cell carcinoma. Biochem Mol Med 54:53–58
7. Izuishi K, Yamamoto Y, Mori H et al (2014) Molecular mechanisms of [18F]fluorodeoxyglucose accumulation in liver cancer. Oncol Rep 31:701–706
8. Ishimori T, Saga T, Mamede M, Kobayashi H, Higashi T, Nakamoto Y, Sato N, Konishi J (2002) Increased 18F-FDG uptake in a model of inflammation: concanavalin A-mediated lymphocyte activation. J Nucl Med 43:658–663
9. Strauss LG (1996) Fluorine-18 deoxyglucose and false-positive results: a major problem in the diagnostics of oncological patients. Eur J Nucl Med 23:1409–1415
10. Nakamoto Y, Saga T, Ishimori T, Higashi T, Mamede M, Okazaki K, Imamura M, Sakahara H, Konishi J (2000) FDG-PET of autoimmune-related pancreatitis: preliminary results. Eur J Nucl Med 27:1835–1838
11. Shreve PD (1998) Focal fluorine-18 fluorodeoxyglucose accumulation in inflammatory pancreatic disease. Eur J Nucl Med 25:259–264
12. Zhuang H, Pourdehnad M, Lambright ES, Yamamoto AJ, Lanuti M, Li P, Mozley PD, Rossman MD, Albelda SM, Alavi A (2001) Dual time point 18F-FDG PET imaging for differentiating malignant from inflammatory processes. J Nucl Med 42:1412–1417
13. Cheng G, Torigian DA, Zhuang H, Alavi A (2013) When should we recommend use of dual time-point and delayed time-point imaging techniques in FDG PET? Eur J Nucl Med Mol Imaging 40:779–787

14. Liu RS, Chou TK, Chang CH, Wu CY, Chang CW, Chang TJ, Wang SJ, Lin WJ, Wang HE (2009) Biodistribution, pharmacokinetics and PET imaging of [(18)F]FMISO, [18F]FDG and [18F]FAc in a sarcoma- and inflammation-bearing mouse model. Nucl Med Biol 36:305–312
15. Tsuji AB, Kato K, Sugyo A, Okada M, Sudo H, Yoshida C, Wakizaka H, Zhang MR, Saga T (2012) Comparison of 2-amino-[3-(1)(1)C]isobutyric acid and 2-deoxy-2-[(1)(8)F]fluoro-D-glucose in nude mice with xenografted tumors and acute inflammation. Nucl Med Commun 33:1058–1064
16. Kaneko K, Sadashima E, Irie K et al (2013) Assessment of FDG retention differences between the FDG-avid benign pulmonary lesion and primary lung cancer using dual-time-point FDG-PET imaging. Ann Nucl Med 27:392–399
17. Yamada S, Kubota K, Kubota R et al (1995) High accumulation of fluorine-18-fluorodeoxyglucose in turpentine-induced inflammatory tissue. J Nucl Med 36:1301–1306
18. Kim SJ, Lee JS, Im KC, Kim SY, Park SA, Lee SJ, Oh SJ, Lee DS, Moon DH (2008) Kinetic modeling of 3′-deoxy-3′-18F-fluorothymidine for quantitative cell proliferation imaging in subcutaneous tumor models in mice. J Nucl Med 49:2057–2066
19. Satomi T, Ogawa M, Mori I, Ishino S, Kubo K, Magata Y, Nishimoto T (2013) Comparison of contrast agents for atherosclerosis imaging using cultured macrophages: FDG versus ultrasmall superparamagnetic iron oxide. J Nucl Med 54:999–1004
20. Longo DL, Bartoli A, Consolino L, Bardini P, Arena F, Schwaiger M, Aime S (2016) In vivo imaging of tumor metabolism and acidosis by combining PET and MRI-CEST pH imaging. Cancer Res 76:6463–6470
21. Behrooz A, Ismail-Beigi F (1997) Dual control of glut1 glucose transporter gene expression by hypoxia and by inhibition of oxidative phosphorylation. J Biol Chem 272:5555–5562
22. Airley R, Loncaster J, Davidson S, Bromley M, Roberts S, Patterson A, Hunter R, Stratford I, West C (2001) Glucose transporter glut-1 expression correlates with tumor hypoxia and predicts metastasis-free survival in advanced carcinoma of the cervix. Clin Cancer Res 7:928–934
23. Yasuda S, Arii S, Mori A, Isobe N, Yang W, Oe H, Fujimoto A, Yonenaga Y, Sakashita H, Imamura M (2004) Hexokinase II and VEGF expression in liver tumors: correlation with hypoxia-inducible factor 1 alpha and its significance. J Hepatol 40:117–123
24. Gautier-Stein A, Soty M, Chilloux J, Zitoun C, Rajas F, Mithieux G (2012) Glucotoxicity induces glucose-6-phosphatase catalytic unit expression by acting on the interaction of HIF-1alpha with CREB-binding protein. Diabetes 61:2451–2460
25. Hustinx R, Smith RJ, Benard F, Rosenthal DI, Machtay M, Farber LA, Alavi A (1999) Dual time point fluorine-18 fluorodeoxyglucose positron emission tomography: a potential method to differentiate malignancy from inflammation and normal tissue in the head and neck. Eur J Nucl Med 26:1345–1348
26. Shinya T, Fujii S, Asakura S, Taniguchi T, Yoshio K, Alafate A, Sato S, Yoshino T, Kanazawa S (2012) Dual-time-point F-18 FDG PET/CT for evaluation in patients with malignant lymphoma. Ann Nucl Med 26:616–621
27. Xiu Y, Bhutani C, Dhurairaj T, Yu JQ, Dadparvar S, Reddy S, Kumar R, Yang H, Alavi A, Zhuang H (2007) Dual-time point FDG PET imaging in the evaluation of pulmonary nodules with minimally increased metabolic activity. Clin Nucl Med 32:101–105
28. Laffon E, de Clermont H, Begueret H, Vernejoux JM, Thumerel M, Marthan R, Ducassou D (2009) Assessment of dual-time-point 18F-FDG-PET imaging for pulmonary lesions. Nucl Med Commun 30:455–461
29. Matthies A, Hickeson M, Cuchiara A, Alavi A (2002) Dual time point 18F-FDG PET for the evaluation of pulmonary nodules. J Nucl Med 43:871–875
30. Lan XL, Zhang YX, Wu ZJ, Jia Q, Wei H, Gao ZR (2008) The value of dual time point 18F-FDG PET imaging for the differentiation between malignant and benign lesions. Clin Radiol 63:756–764